



HORIZON 2020

The EU Framework Programme for Research and Innovation

H2020-EO-1-2014

# Spatial assessment of heat storage flux ( $\Delta Q_s$ )

Deliverable D5.1



## LEAD AUTHOR

Fredrik Lindberg (UoG)

## DATE

1 January 2016

## ISSUE

1.0

## GRANT AGREEMENT

no 637519

## DISSEMINATION LEVEL

PU

## AUTHORS

Frans Olofson (UoG), Sue Grimmond (UoR)

## CONTRIBUTORS

Nektarios Chrysoulakis (FORTH), Zina Mitraka (FORTH)

## CONTENTS

1	Introduction .....	2
1.1	Purpose of the document .....	2
1.2	Definitions and acronyms.....	2
2	Project Overview .....	4
3	Spatial Assessment of Storage Heat Flux .....	6
3.1	Concept and approach .....	6
3.2	ESTM input data.....	7
3.2.1	Urban morphology.....	9
3.2.2	Surface temperature.....	9
3.2.3	Indoor air temperature.....	9
4	Model sensitivity.....	10
4.1	Datasets.....	10
4.2	Sensitivity results .....	11
4.2.1	Urban morphology.....	11
4.2.2	Element temperatures.....	12
4.2.3	Material characteristics.....	13
4.3	Conclusions from sensitivity tests.....	14
5	City scale heat storage flux .....	15
5.1	Model setup and input data.....	15
5.2	Initial results.....	18
6	Planned activities.....	19
7	Acknowledgements .....	20
8	References .....	20
9	Appendices .....	22

## 1 INTRODUCTION

### 1.1 Purpose of the document

This document outlines the methods being explored to determine the storage heat flux for urban areas within the URBANFLUXES project. This term is one component within the surface energy balance. The goal of URBANFLUXES is to determine the energy balance fluxes at a resolution of 100 m across an urban area using remote sensing techniques.

### 1.2 Definitions and acronyms

#### Acronyms

$a$	sine function amplitude
$\alpha_s$	solar elevation angle (rad)
DEM	Digital Elevation Model
DSM	Digital Surface Model
EO	Earth Observation
ESTM	Elemental Surface Temperature Method
$f$	element fraction
$FOV_{sat}$	satellite Field Of View (rad)
GIS	Geographical Information System
$z_H/W$	height-to-width ratio
ibld	internal building (floor, ceiling and non-outer walls)
$k$	material thermal conductivity ( $W\ m^{-1}\ K^{-1}$ )
$K_{\downarrow}$	incoming solar radiation ( $W\ m^{-2}$ )
LCZ	Local Climate Zone
LST	Land Surface Temperature (K)
$n_{room}$	number of rooms per floor
PAI	Plan Area Index (the same as $f_{roof}$ )
$Q^*$	net all-wave radiation ( $W\ m^{-2}$ )
$\Delta Q_s$	net storage heat flux ( $W\ m^{-2}$ )
$\rho C$	volumetric heat capacity ( $J\ m^{-3}\ K^{-1}$ )
svf	sky view factor
$t_{day}$	time of day (decimal hours)
$t_{elev}$	time of sunrise (decimal hours)
$t_{mid}$	time during the day with maximum outdoor air temperature (decimal hours)
$T_b$	brightness temperature (K)
$T_{iair}$	indoor air temperature (K)
$T_{oair}$	outdoor air temperature (K)
$T_{oair\ spline}$	splined outdoor air temperature (K)
$T_{surf}$	surface temperature (K)
$T'_{surf}$	gap-filled surface temperature (K)



---

$T_{\text{surf spline}}$	splined surface temperature (K)
UMEP	Urban Multi-scale Environmental Predictor
URBANFLUXES	URBan ANthropogenic heat FLUX from Earth observation Satellites
WP	Work Package
$x$	element thickness (m)
$z_H$	mean building height (m)

---

## 2 PROJECT OVERVIEW

---

The anthropogenic heat flux ( $Q_F$ ) is the heat flux resulting from vehicular emissions, space heating and cooling of buildings, industrial processing and the metabolic heat release by people. Both urban planning and Earth system science communities need spatially disaggregated  $Q_F$  data, at local (neighbourhood, or areas larger than the order of 100 m x 100 m) and city scales. Such information is practically impossible to derive by point *in-situ* fluxes measurements, while satellite remote sensing is a valuable tool for estimating Urban Energy Budget (UEB) parameters exploiting Earth Observation (EO) data. While the estimation of  $Q_F$  spatial patterns by current EO systems is a scientific challenge, the major challenge lies on the innovative exploitation of the Copernicus Sentinels synergistic observations to estimate the spatiotemporal patterns of  $Q_F$  and all other UEB fluxes.

The main goal of URBANFLUXES is to investigate the potential of EO to retrieve  $Q_F$ , supported by simple meteorological measurements. The main research question addresses whether EO is able to provide reliable estimates of  $Q_F$  for the time of the satellite acquisition. URBANFLUXES answers this question by investigating the potential of EO to retrieve  $Q_F$  spatial patterns, by developing a method capable of deriving  $Q_F$  from current and future EO systems. URBANFLUXES aims to develop an EO-based methodology easily transferable to any urban area and capable of providing  $Q_F$  benchmark data for different applications. URBANFLUXES is expected to increase the value of EO data for scientific analyses and future emerging applications (such as urban planning and local/regional level climate change mitigation/adaptation), by exploiting the improved data quality, coverage and revisit times of the Copernicus Sentinels data. To this end, the specific objectives of the project are:

- to improve the accuracy of the radiation balance spatial distribution calculation;
- to develop EO-based methods to estimate the flux of heat storage in the urban fabric, as well as the turbulent sensible and latent heat fluxes at local scale;
- to employ energy budget closure to estimate the anthropogenic heat flux patterns;
- to specify and analyse the uncertainties associated with the derived products;
- to evaluate the products by comparisons with  $Q_F$  estimations by independent methods;
- to improve the understanding of the impact of  $Q_F$  on urban climate; and to communicate this understanding to the urban planning community, which will in turn lead to a better understanding of what new knowledge is needed on the ground;
- to exploit Sentinels 2 and 3 synergistic observations to retrieve UEB fluxes at the local scale, with the frequency of the Sentinel 3 series acquisitions.
- to standardise the resulting products, and by organizing an effective dissemination mechanism, to enhance their use by urban planners and decision makers in cities, as well as by EO scientists, Earth system modellers and urban climatologists.

The duration of URBANFLUXES is three years and it is divided into two main phases: during the 1<sup>st</sup> Phase an analysis method is being developed to estimate  $Q_F$  spatial patterns using currently available satellite data; during the 2<sup>nd</sup> Phase the developed method will be adapted to Sentinels synergy to derive  $Q_F$  spatiotemporal patterns. Three different urban areas are selected in URBANFLUXES as case studies: a highly urbanized mega city (London); a typical central European medium size city, that requires a substantial amount of energy for heating (Basel); and a smaller, low latitude Mediterranean city that requires a substantial amount of energy for cooling (Heraklion). The project uses a Community of Practice (CoP) approach, which means that in the case studies, local stakeholders and scientists meet on a regular basis to learn from each other and to make clear what aspects are important for the future users of the URBANFLUXES products.

URBANFLUXES is expected to generate a novel analysis method for estimation of UEB components from Copernicus data, enabling its integration into applications and operational services; for example to: develop rules of thumb for density and green space ratio, distinguish between insulated and non-insulated buildings and evaluate the implementation of climate change mitigation technologies, such as solar-screening and green-belting.

Despite its local importance,  $Q_F$  is omitted from climate models simulations. Observations of global temperature evolution indicate a pronounced warming over the last 150 years, with an increase in the occurrence of heat waves. The added value and benefit expected to emerge from URBANFLUXES is therefore related to quality of life, because it is expected to improve our understanding of the contribution of  $Q_F$  to heat wave intensity and thus to allow insight into strategies for mitigation.  $Q_F$  estimates are needed for all cities to be able to document the magnitude of the fluxes effects on urban climate so that the impact of  $Q_F$  can be included in climate modelling. URBANFLUXES is therefore expected to advance the current knowledge of the impacts of  $Q_F$  on urban heat island and hence on urban climate, and consequently on energy consumption in cities. This will lead to the development of tools and strategies to mitigate these effects, improving thermal comfort (social benefit) and energy efficiency (economic benefit). The long term operation of the Sentinels series guarantees the future supply of satellite observations, providing the means for the development and realization of the URBANFLUXES methodology.

URBANFLUXES is expected to support sustainable planning strategies relevant to climate change mitigation and adaptation in cities, because knowledge of  $Q_F$  spatio-temporal patterns is important for urban planning (e.g. to reduce or prevent  $Q_F$  hot spots), health (e.g. to estimate the impact on thermal comfort) and future proofing (e.g. to plan and implement interventions towards  $Q_F$  reduction in these areas). Planning tools, such as Urban Climatic Maps and Climatope Maps, should be enriched with information on  $Q_F$  patterns. Mapping provides visualization of assessments of these phenomena to help planners, developers and policy makers make better decisions on mitigation and adaptation.

## 3 SPATIAL ASSESSMENT OF STORAGE HEAT FLUX

### 3.1 Concept and approach

The storage heat flux of an urban canopy is approximately 2 - 6 times larger than for non-urban canopies (Oke, 1987). The net storage heat flux ( $\Delta Q_s$ ) is the net flow of heat stored within the urban volume, i.e. the air, trees, buildings, ground, etc. In urban areas, the net heat stored in the canopy is a relatively large fraction of  $Q^*$  (Nunez and Oke, 1977; Grimmond and Oke, 1999). Directly evaluating  $\Delta Q_s$  in the urban canopy is very difficult (Meyn and Oke, 2009).

There are several methods to determine  $\Delta Q_s$  (Offerle et al., 2005; Roberts et al., 2006). An approach that is being explored for URBANFLUXES is the Element Surface Temperature Method (ESTM) (Offerle et al., 2005) which reduces the three-dimensional urban volume to four 1-d elements (i.e. building roofs, walls, and internal mass and ground (road, vegetation, etc)). The flux is calculated as (Offerle et al., 2005):

$$\Delta Q_s = \sum_i \frac{\Delta T_i}{\Delta t} \rho_i C \Delta x_i f_{\text{roof}} \quad (1)$$

where  $\Delta T_i/\Delta t$  is the rate of temperature change over the period for each element  $i$ ,  $\rho C$  is the volumetric heat capacity,  $\Delta x$  is the element thickness and  $f_{\text{roof}}$  is fraction of roof, i.e. the plan area index. So,  $\Delta x_i f_{\text{roof}}$  is the total element volume over the plan area, for each element  $i$ . If the average internal element temperature is not directly measured:

$$\rho C \frac{\partial T}{\partial t} = -\frac{\partial Q}{\partial x} = -\frac{\partial}{\partial x} \left( -k \frac{\partial T}{\partial x} \right) \quad (2)$$

where  $Q$  is the heat flux through the surface and  $k$  is the thermal conductivity. For the inside surfaces of the roof and walls, and both surfaces for the internal mass (floors, internal walls), the surface temperature of element  $i$  is determined by setting the conductive heat transfer out of (in to) the surface equal to the radiative and convective heat losses (gains), as described by Offerle et al. (2005).

Other methods to assess the storage heat flux include:

- 1) OHM: Objective Hysteresis Method (Grimmond et al., 1991; Grimmond and Oke, 1999)
- 2) RES: Residual – determination of the storage heat flux from the residual of the surface energy balance (Offerle et al., 2005)
- 3) TEB: Town Energy Balance model (Masson, 2000), an urban land surface model

Offerle et al. (2005) compared the ESTM model with RES, OHM and TEB using measurements made in Łódź, Poland during 2002. They concluded that it was possible to determine reasonable  $\Delta Q_s$  values based on a representative surface temperature sampling.

The objectives of the work reported here are to:

- 
- (1) Document the methods for the application of the ESTM.
  - (2) Assess the sensitivity of the ESTM methods.
  - (3) Apply the ESTM method for one day in Basel (one of the three study areas of Basel).

### 3.2 ESTM input data

The surface morphology and material characteristics are essential parameters in the ESTM scheme (Table 1). The following sections outline the methods used to determine the inputs so the ESTM algorithm can be applied at a range of different scales.

**Table 1.** Inputs required for the ESTM storage heat flux model. The values and sources of data are reported for three cities where ESTM is used: Łódź (all data from Offerle et al. 2005); London (data from University of Reading LUMA,) Basel (data from University of Basel).

	Łódź	London	Basel	Methods/Details
<b>Data period</b>				
	19 July - 29 August, 2002	1 - 30 June, 2015	30 August, 2015	
<b>Surface temperatures (<math>T_{surf}</math>)</b>				
number of sensors	1	5	1	
measurement method	T-type thermocouple attached to roof surface	Optris IR camera	Landsat 8 satellite	
<b>Outdoor air temperature (<math>T_{oair}</math>)</b>				
measurement height (m)	37	125	27.5	
<b>Indoor air temperature (<math>T_{iair}</math>)</b>				
data source	measured	Equation 5	Equation 5	Section 2.2.3
<b>Surface Characteristics</b>				derived from DSM/DEM
plan area of roof	0.3	0.36		
plan area of ground (impervious and vegetation)	0.7	0.64		
fraction of building external wall surface	0.8	1.08	variable	Appendix A1
fraction building internal surface (walls, ceilings/floors)	2.1	3.85	variable	Appendix A1
mean building height (m)	17	22.9	variable	Section 2.2.1
height-to-width ratio (section 2.2.1)	0.75	0.84	variable	used to calculate svf
number of floors	4	6	variable	calculated from $z_H$
number of rooms per floor	10	10	20	estimation
area	500 m x 500 m	230 m x 240 m	5 km x 5 km	

### 3.2.1 Urban morphology

The street canyon (Nunez and Oke, 1977) is a widely used basic geometric unit to describe the urban area. It consists of a mean building height ( $z_H$ ) and width ( $W$ ). To calculate these morphological parameters it is necessary to simplify “real” 3-d urban morphology into a 1-d infinitively long street canyon which has roof, wall and ground facets. There are a variety of different techniques for this 3-d to 1-d transformation (Lindberg et al., 2015). Here we use Martilli’s (2009) approach which ensures conservation of heat and momentum. The fractions of the three street canyon facets are set to be the same as the “real morphology”, so that:

$$\frac{z_H}{W} = \frac{f_{\text{wall}}}{2(1-f_{\text{roof}})} \quad (3)$$

where  $f_{\text{wall}}$  is the fraction of the wall area relative to the total horizontal area. For details see Martilli (2009) or Lindberg et al. (2015) and Appendix A1. The parameters are then derived from high resolution digital surface models (DSM).

The fraction of internal building surface elements ( $f_{\text{ibld}}$ ) depends on the fractions of wall ( $f_{\text{wall}}$ ) and roof ( $f_{\text{roof}}$ ) and on the mean building height ( $z_H$ ) and the number of rooms per floor ( $n_{\text{room}}$ ).

$$f_{\text{ibld}} = \left(2 \left(1 - \frac{1}{n_{\text{room}}}\right)\right) f_{\text{wall}} (f_{\text{roof}}, \frac{z_H}{W}) + \left(\left[\frac{z_H}{3.1} - \frac{1}{2}\right] - 1\right) f_{\text{roof}} \quad (4)$$

For a limited number of rooms per floor, the internal building fraction increases rapidly but as the number grows so does the wall fraction. Beyond ten rooms per floor, the change of the contribution of internal building surface to the sum of the total urban surface area is small.

### 3.2.2 Surface temperature

Surface temperature determined remotely is a product of the brightness temperature ( $T_b$ ) and the surface emissivity. The component surfaces in a satellite pixel field of view ( $\text{FOV}_{\text{sat}}$ ) influences the  $T_b$  reported by the satellite sensor. However,  $\text{FOV}_{\text{sat}}$  does not view the complete surface (Voogt and Oke, 2003) (this is explored in section 3.2.2). The temporal resolution of satellite-derived temperatures with high spatial resolution is insufficient to run the ESTM-scheme, therefore data from ground and satellite sources are used to estimate  $\Delta Q_s$ .

At best (i.e. assuming no cloud cover), one high spatial resolution (100 m or less) satellite acquisition every six hours will be available in the URBANFLUXES project. The ESTM-scheme has a time step of minutes requiring a continuous gap filled forcing data, thus allowing the rate of change in surface temperature to be used in equation 1 at the time of the satellite passage.

### 3.2.3 Indoor air temperature

The temperature of internal building elements is mainly controlled by the indoor air temperature. If this variable is not accessible a model can be used. Here an equation was developed to mimic day and night average indoor air temperature data used by Georgitisi

(2011). A diurnally varying indoor air temperature with a sinusoidal variation around a base value of 22.5 °C with a minimum at 04:00 and a maximum at 16:00 was used. In addition, the indoor air temperature was modulated so the base value increases as outdoor air temperature ( $T_{\text{air}}$ ) increases, and vice versa.

$$T_{\text{air}} = \left(1 + \frac{T_{\text{air}} - 22.5}{5 \cdot 22.5}\right) \left(22.5 + 0.4 \sin\left(\frac{3\pi}{4} t_{\text{day}}\right)\right) \quad (5)$$

The time of the day ( $t_{\text{day}}$ ) is expressed in decimal hours. The resulting diurnal peak-to-peak indoor air temperature amplitude typically falls within the 1 - 5 °C range. In the results presented in sections 3 and 4, this method to calculate the indoor air temperature was used for London and Basel, while measured indoor air temperature was used for Łódź.

## 4 MODEL SENSITIVITY

Sensitivity studies are performed to identify the relative importance of different parameters and variables to the ESTM scheme. This informs an understanding of the spatial assessment of storage heat flux.

### 4.1 Datasets

Two data sets are used for the sensitivity analyses (a) the original ESTM-scheme data set from Łódź, Poland (Offerle et al., 2005) and (b) a high resolution dataset from London, UK (Table 1).

In Łódź, measurements in a university building (51.77° N, 19.45° E) consisted of 15 min averages of: outdoor air temperature, indoor air temperature and one roof surface temperature. The surface temperature measurements were made with a T-type thermocouple probe, attached to the university building roof. The area analysed (500 m x 500 m, around an eddy covariance flux tower) was in the central business district with a couple of small parks. The street canyons are lined with (typically) three to five storied buildings and occasional trees (Offerle, 2003). The results presented (Sections 3.2.1 and 3.2.3) are based on observations for the period 19 July - 29 August, 2002.

The London observations were made in the Barbican district in the city of London (51.52° N, -0.09° E), an area with 10 storey buildings interspersed with three 42 storied buildings and two small parks. The outer building material is almost exclusively concrete and glass. Surface brightness temperatures (Optris Pi 160 thermal camera) and air temperature (Davis Vantage Pro 2 plus, aspirated) were sampled at 1 min and 5 s respectively. The temperatures used are 15 minute averages. Five element surfaces (Figure 1): one ground, three walls (N, E, S facing) and one roof surface were analysed. They span an area of 230 m x 240 m. The indoor air temperatures were modelled (Section 2.2.3).

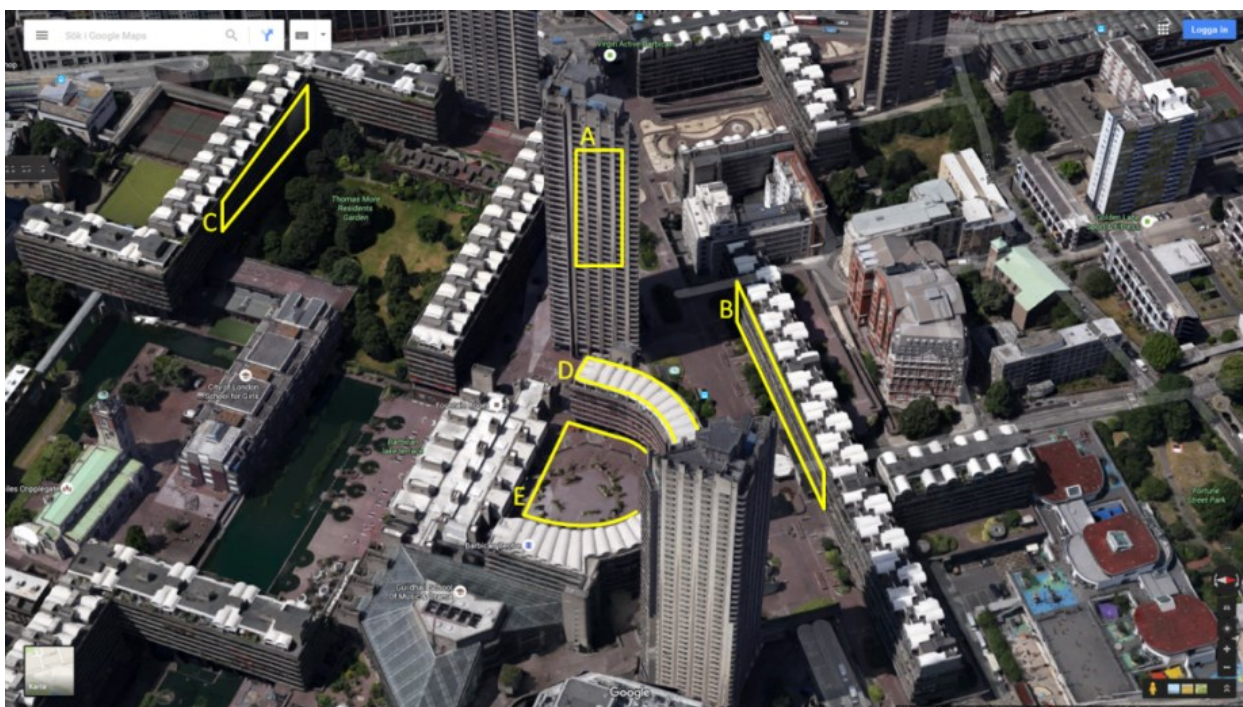


**Figure 1.** Barbican study area (London) with five IR camera sampled facets. A: east wall, B: south wall, C: north wall, D: roof and E: ground. Image source: Google maps.

Digital Surface Models (DSMs) were used to calculate fractions of roof, wall and ground together with height-to-width ratio and sky-view-factors (Section 2.2.1 and Appendix A1). The indoor building geometry has an idealised layout with two rows of equally sized rooms separated by a corridor, for each floor.

## 4.2 Sensitivity results

### 4.2.1 Urban morphology

Within a city the morphology (e.g. heights, canyon widths) varies considerably. The Łódź dataset was used to investigate how the mean building height and the associated wall area influences the heat storage. When the mean building height is varied from 5 to 100 m, with a constant canyon width, the ESTM modelled  $\Delta Q_{s, wall}$  scales linearly with the building height (see Equation 3), while the ground and roof fractions remain the same. For example, when the mean building height reaches approximately 25 m the wall fraction exceeds the ground and roof fractions combined (Figure 2). The mean building height is identified as an important parameter in the ESTM model.

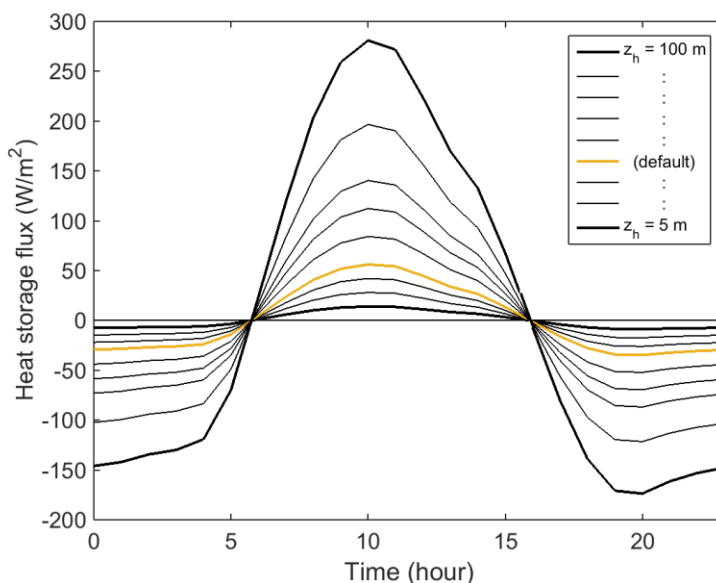


**Figure 2.** Diurnal hourly averages wall storage heat flux as a function of mean building height (walls heights: 5, 10, 15, 20, 30, 40, 50, 70 and 100 m) for Łódź. The yellow curve represents the morphological conditions presented in Table 1 and Table A1.

#### 4.2.2 Element temperatures

The ESTM model can be run in three different surface temperature modes:

- i) all facets have the same temperature,
- ii) roof, wall and ground have individual temperatures, and
- iii) roof, the four cardinal wall directions and ground have their individual temperatures.

In an urban setting, typically the roofs heat up most intensely in the morning while the ground and some of the walls are likely to be in shadow, and therefore have a slower heating process. The walls that heat up (cool down) first (last) are dependent on the orientation and time of the day. East walls heat up first and west walls last. This general pattern is modulated by the unique morphology of the city and to some extent the material thermal properties.

When individual surface temperatures are used for roof, wall and ground, the peaks in heat uptake can be seen to vary between the facets (Figure 3a). The lower (absolute) flux for the roof is probably a result of its white colour high albedo of 0.7 (Hogenhout, 2010). The wall component peaks first, which can be attributed to the magnitude of glazing (50%) and the resulting comparatively low volumetric heat capacity (Table A1). When all surfaces have the same temperature (the mean of the roof and ground temperatures), which may be similar to what a nadir sensing satellite would see, the total heat storage flux maximum increases from around  $100 \text{ W m}^{-2}$  to almost  $120 \text{ W m}^{-2}$  (Figure 3b). The way surface temperatures are treated

can have some effect on the amplitude of the total heat storage flux and the diurnal pattern. However, the differences between the two ESTM model modes are more evident for the phase of the different components and their respective magnitudes (compare for example  $Q_{S_{wall}}$  in Figure 3a and b).

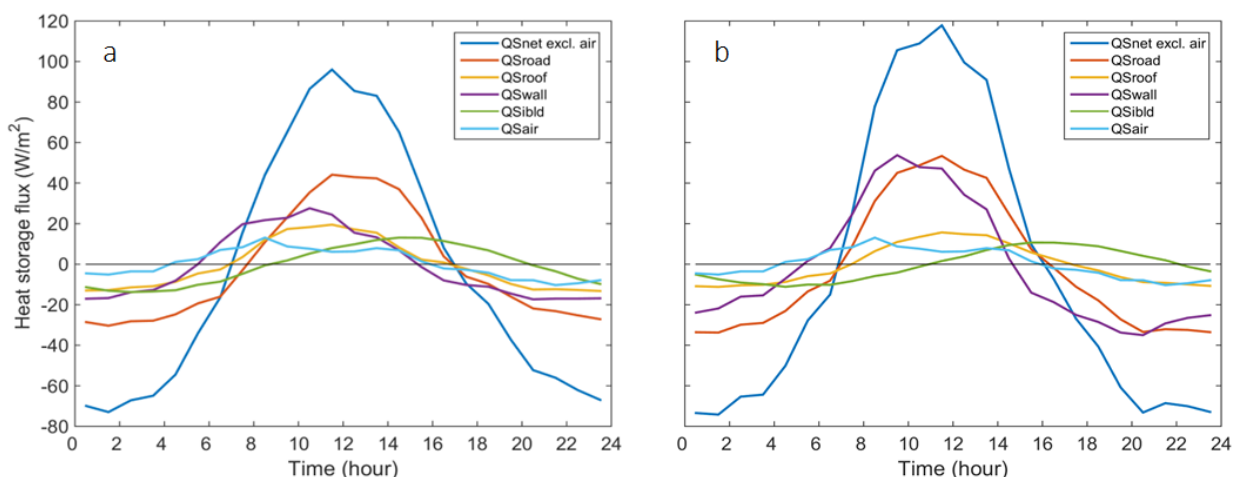


**Figure 3.** Diurnal hourly average storage heat flux and components (London, June 2015) when (a) different surface temperatures are used for the individual facets and (b) when the surface temperature (average of roof and ground) is set equal for all facets. Indoor (ibld) and air temperatures are also used. The different storage heat fluxes are divided into: ground ( $Q_{S_{road}}$ ), roof ( $Q_{S_{roof}}$ ), wall ( $Q_{S_{wall}}$ ), internal building ( $Q_{S_{ibld}}$ ), outdoor air ( $Q_{S_{air}}$ ) and the sum of ground, roof, wall and internal building ( $Q_{S_{net\ excl.\ air}}$ ).

The diurnal temperature variation of indoor building elements is small compared to that of the other urban surface elements. The internal building heat storage flux component typically makes up around one tenth or less of the total. Overall, the characteristics of the indoor elements and their associated heat storage present a minor influence on the total net heat storage flux.

#### 4.2.3 Material characteristics

The thermal properties of a material determine, for a certain temperature difference, how much heat can be exchanged and the rate of the heat exchange. In the ESTM model, these properties are described by the volumetric heat capacity ( $\rho C$ ) and the thermal conductivity ( $k$ ), which are the variables used to calculate the heat conduction through roof, wall and ground. The urban fabric typically has a range of different materials, with different thermal properties (Appendix A3).

Figure 4 shows the wall heat storage component, for the Łódź dataset, for five different construction materials – brick, concrete, glass, stone and wood. The wall surface element is

made up of three layers, each 10 cm thick and with its own heat capacity and thermal conductivity. For simplicity, only the outermost layer properties are changed in the comparison. The thermal conductivity exhibits a broad span, from  $0.19 \text{ W m}^{-1} \text{ K}^{-1}$  for wood to  $2.19 \text{ W m}^{-1} \text{ K}^{-1}$  for stone. The volumetric heat capacities fall between approximately  $1.5$  and  $1.6 \text{ MJ m}^{-3} \text{ K}^{-1}$ , except for stone with a value of  $2.25 \text{ MJ m}^{-3} \text{ K}^{-1}$  (Hutcheon and Handegord, 1989; Offerle et al., 2005; Roberts et al., 2006). The rest of the parameters are set to the default values, listed in Table 1. Different materials can cause large differences in heat storage fluxes, e.g. a fivefold increase from wood to stone. The different urban elements are normally built up by several layers of varying materials. The set of urban materials, including the ground element, and their respective thicknesses are identified as important parameters in the ESTM model.

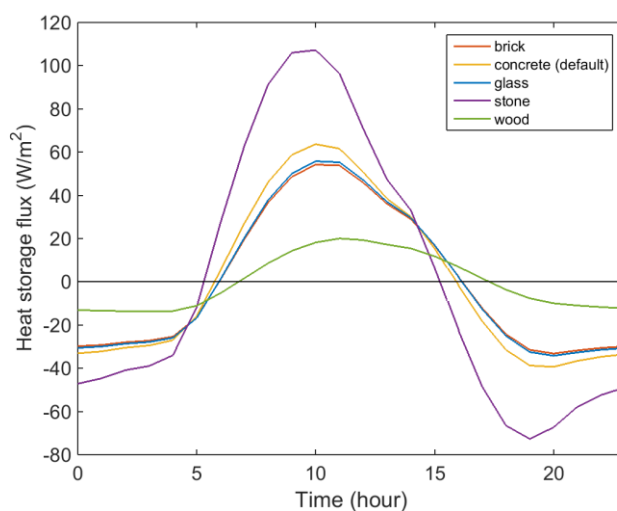


**Figure 4.** Impact of surface material properties on the diurnal hourly wall storage heat flux. The yellow curve shows the Łódź default case and the other curves were calculated with material thermal properties from Roberts et al. (2006) and Hutcheon and Handegord (1989).

### 4.3 Conclusions from sensitivity tests

From the sensitivity tests undertaken so far of the ESTM model, the following conclusions are drawn:

- 1) There is low sensitivity to the internal air temperatures, so detailed knowledge is not critical.
- 2) The method of averaging component surface temperatures has a large influence, so it needs careful consideration.
- 3) The results are sensitive to building dimensions used in the calculations, so care needs to be taken to the method used to assign these values.
- 4) The parameters assigned in the model to describe thermal responses of building material have a large effect. Ensuring these are appropriate is important.

## 5 CITY SCALE HEAT STORAGE FLUX

Using satellite information in conjunction with GIS-derived surface information, it is possible to examine spatial variations of  $\Delta Q_s$  across an urban area. Here, an example from Basel, Switzerland, is demonstrated.

### 5.1 Model setup and input data

To consider the spatial variations of the storage heat flux a 5 km x 5 km area of central Basel (Figure 5) was used as the study area. A high resolution Digital Surface Model (DSM) was used to derive the various morphometric parameters needed (see Table 1). The spatial variation of  $\Delta Q_s$  was calculated using a 100 m x 100 m grid.

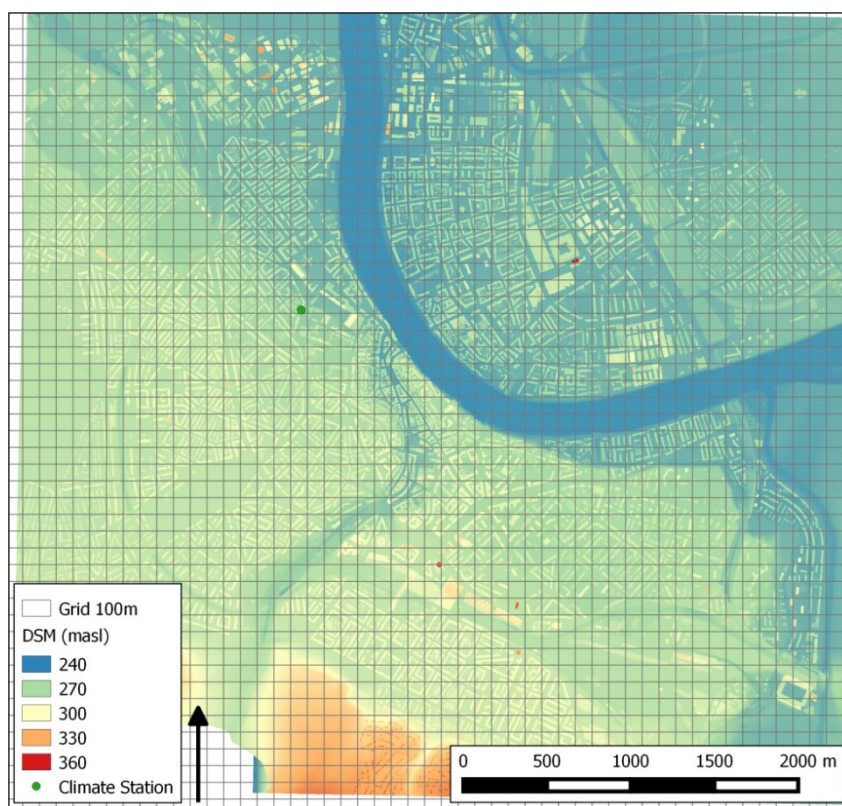


**Figure 5.** Central Basel, Switzerland 1m resolution digital surface model (DSM), showing heights in metres above sea level, on a 5 km x 5 km grid with a grid cell size of 100 m x 100 m. Source: Basel city authorities, 2008.

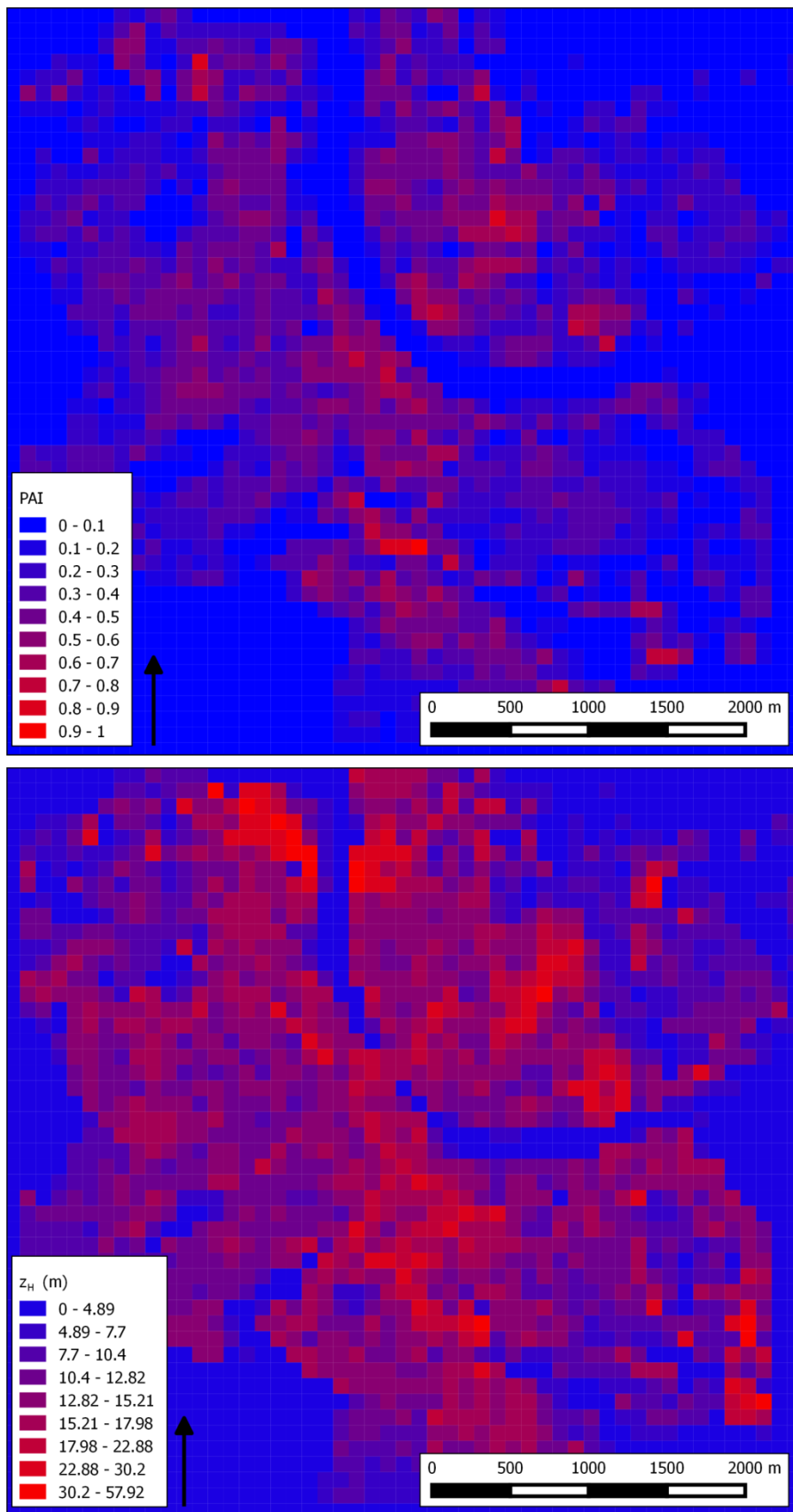


**Figure 6.** Central Basel (top) plan area index and (bottom) mean building height calculated from a 1 m resolution DSM and downscaled to 100 m. Source: Basel city authorities and Basel University.

From the DSM, the required input morphological parameters, roof fraction ( $f_{roof}$ ), mean building height ( $z_H$ ), wall fraction ( $f_{wall}$ ) and height-to-width ratio ( $z_H/W$ ), were calculated as described in section 2.2.1. The reference height ( $z_{ref}$ ) is defined as twice the mean building height. The fraction of internal building elements ( $f_{ibld}$ ) was calculated according to section 2.2.1, with the number of rooms per floor ( $n_{room}$ ) set to 20. The plan area index and mean building height covering the study area are shown in Figure 6. The building fraction is higher in certain central parts of the city where some of the highest mean building heights also are found.

Surface temperature was aggregated to the 100 m grid from a Landsat 8 scene acquired on 30 August, 2015 at 1116 CET (Figure 8). This day was characterised by clear and warm weather. The brightness temperatures are corrected for emissivity and for atmospheric absorption after Sobrino et al. (2004), using a simple NDVI approach. The URBANFLUXES sensor network was not operational at the time of the satellite overpass. Therefore, a single air temperature (27.5 m agl) from a climate station in the central part of the city (Figure 6) was used. The indoor air temperature was modelled as described in section 2.2.3.

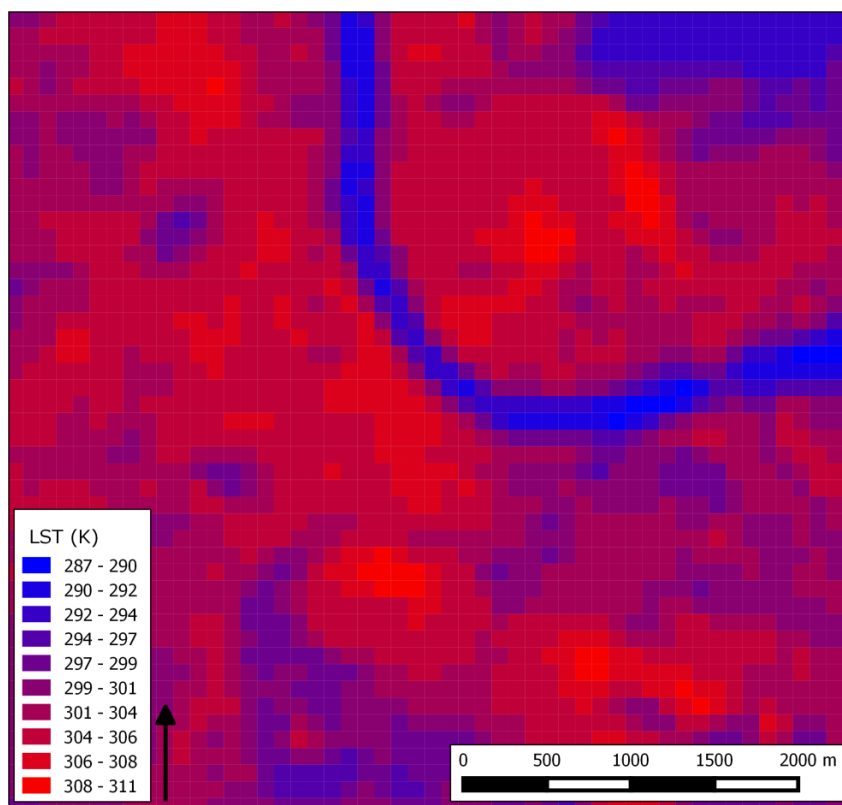


**Figure 7.** Land surface temperature (LST) in central Basel on the 30 August, 2015 at 1116 CET at 100 m spatial resolution. Source: Landsat 8 (<http://lpdaac.usgs.gov/>).

---

The ESTM-scheme was set-up to run from midnight to midnight for the day of the satellite overpass. To be able to run the model continuously and obtain surface temperature change, a surface temperature time series has to be calculated. This was achieved by utilizing the recorded satellite surface temperature together with air temperature according to the sine function method described in Appendix A2. Due to lack of grid specific material properties or LCZs the same values as in the dataset for Łódź, a typical central European medium size city like Basel, were used. The same set of thermal properties and surface layer thicknesses was used for all the grid cells. The storage heat flux input parameters for Basel are presented in Table 1.

## 5.2 Initial results

Figure 8 shows the estimated  $\Delta Q_s$  for the Landsat 8 scene used (30 August, 2015 at 1116 CET). In this example, the spatial pattern is affected by urban morphology and surface temperatures. Materials, indoor and outdoor air temperature are the same for the whole model domain. The highest  $\Delta Q_s$  is found in the central parts of the city. This is the densest part of Basel, with the warmest surface temperatures at this time. Cooler areas, with lower building density such as parks and open water, show, as expected, lower  $\Delta Q_s$ . Information on materials would probably accentuate the spatial differences of  $\Delta Q_s$  given dense urban areas tends to include materials such as stone and concrete which have the ability to store more energy and hence increase  $\Delta Q_s$ .

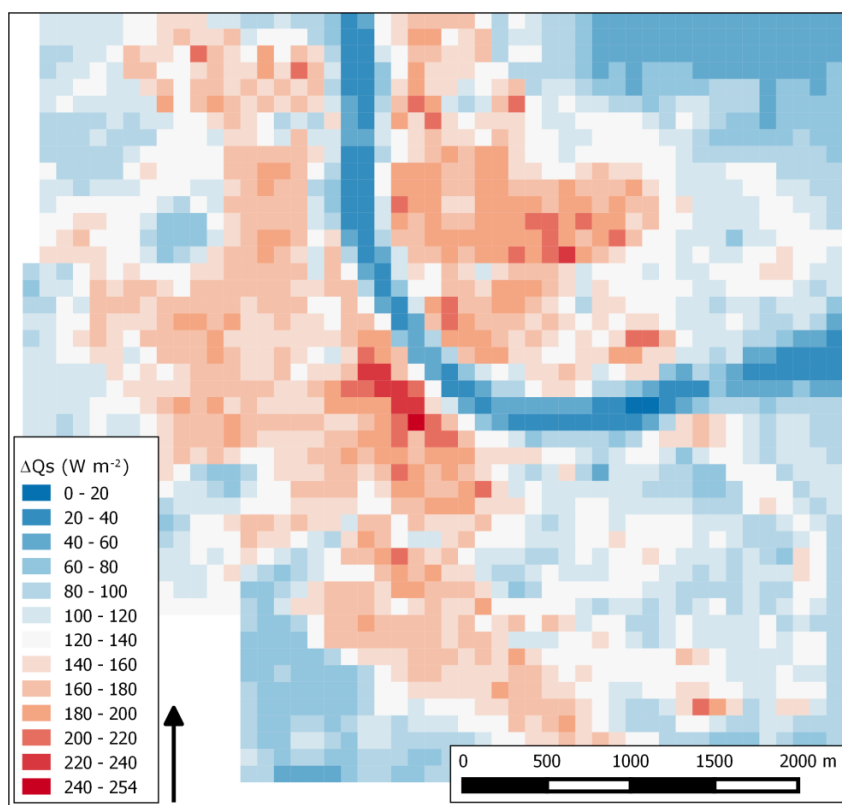


**Figure 8.** Storage heat flux calculated with the ESTM method (30 August, 2015 at 11:16 CET, central Basel, Switzerland) at 100 m spatial resolution.

## 6 PLANNED ACTIVITIES

The initial results of spatially derived storage heat fluxes from the ESTM-scheme will be improved ahead of the next deliverables included in WP5 informed by the sensitivity analyses (section 3). As more information on materials and land use/land cover becomes available, this will be included in the spatial modelling. More work on the study area in London will be performed to investigate further the influence of material properties and wall temperatures on  $\Delta Q_s$  and the possibility to parameterize temperatures not seen by the satellite sensor. WP5 will also pursue work on extrapolating the morphology parameters outside areas where detailed information on urban morphology is not available.

The indoor air temperature model used in this work should be evaluated and compared to existing measured data. Furthermore, the model sensitivity to element thickness needs to be examined.

The next milestone for WP5 will be the Deliverable D5.2 (M18) where a comparison between the ESTM-scheme and other heat storage models will be conducted. This comparison will

---

consider both spatial and temporal perspectives. Other tasks, such as the documentation of the database that includes all derived  $\Delta Q_s$  products, for all case studies (also part of the Deliverable D5.3), will also be prepared.

## 7 ACKNOWLEDGEMENTS

---

The Landsat 8 data was available from the U.S. Geological Survey. The London IR camera surface temperature data was available from University of Reading, LUMA.

## 8 REFERENCES

---

ASHRAE, 2013. *ASHRAE handbook – fundamentals*. American Society of Heating, Refrigerating and Air-Conditioning Engineers, Inc.

Behar, C., 2011. *An Investigation of the Effectiveness of Post-Occupancy Evaluation Techniques in Characterizing Baseline User Satisfaction, Energy Use and Behaviour in Barbican Centre Dwellings*. [thesis]

de Boor, C., 1978. *A Practical Guide to Splines*. Springer-Verlag.

Galeazzi, C., 2010. *The Energy Performance of an Iconic example of Brutalist Architecture in London: a Case Study of the Barbican Residential Towers*. [thesis]

Georgitsi, E., 2011. *Barbican under-floor heating comfort and energy*. [thesis]

Grimmond, C. S. B., Cleugh, H. A. and Oke, T. R., 1991. An objective urban heat storage model and its comparison with other schemes. *Atmos. Environ.* 25B, 311 - 326.

Grimmond, C. S. B. and Oke, T. R., 1999. Heat storage in urban areas: Local-scale observations and evaluation of a simple model. *J. Appl. Meteorol.* 38, 922 - 940.

Hogehout, S., 2010. *Modelling the urban microclimate: A case study of the Barbican Estate in London*. [thesis]

Hutcheon, N. B. and Handegord, G., 1989. *Building science for a cold climate*. Construction Technology Centre Atlantic, Inc.

Lindberg, F., Holmer, B. and Thorsson, S., 2008. SOLWEIG 1.0 – Modelling spatial variations of 3D radiant fluxes and mean radiant temperature in complex urban settings. *Int. J. Biometeorol.* 52:697 - 7134.

Lindberg, F., Grimmond, C. S. B. and Martilli, A., 2015. Sunlit fractions on urban facets - Impact of spatial resolution and approach. *Urban Clim.* 12, 65 - 84.

---

Masson, V., 2000. A physically-based scheme for the urban energy budget in atmospheric models. *Bound.-Layer Meteorol.* 94, 357 - 397.

Martilli, A., 2009. On the derivation of input parameters for urban canopy models from urban morphological datasets. *Bound.-Layer Meteorol.* 130, 301 - 306.

Meyn, S. K. and Oke, T. R., 2009. Heat fluxes through roofs and their relevance to estimates of urban heat storage. *Energy and Build.* 41, 745 - 752.

Mörtstedt, S.-E. and Hellsten, G., 1992. *Data och diagram*. Liber Utbildning AB.

Nunez, M. and Oke, T. R., 1977. The energy balance of an urban canyon. *J. Appl. Meteorol.* 16, 11 - 19.

Offerle, B., 2003. *The energy balance of an urban area: examining temporal and spatial variability through measurements, remote sensing and modelling*. [thesis]

Offerle, B., Grimmond, C. S. B. and Fortuniak, K., 2005. Heat storage and anthropogenic heat flux in relation to the energy balance of a central European city centre. *Int. J. Climatol.* 25, 1405 - 1419.

Oke, T. R., 1987. *Boundary layer climates*. Routledge.

Roberts, S. M., Oke, T. R., Grimmond, C. S. B. and Voogt, J. A., 2006. Comparison of four methods to estimate urban heat storage, *J. Appl. Meteorol. Climatol.* 45, 1766 - 1780.

Sobrino, J. A., Jiménez-Munóza, J. C. and Paolini, L., 2004. Land surface temperature retrieval from LANDSAT TM 5. *Remote Sens. Environ.* 90, 434 - 440.

Voogt, J. A. and Oke, T. R., 2003. Thermal remote sensing of urban climates. *Remote Sens. Environ.* 86, 370 - 384.

## 9 APPENDICES

### A1. Calculation of $f_{\text{wall}}$ and $f_{\text{roof}}$

To derive  $f_{\text{wall}}$  from a vector dataset, the topological structure, as well as the accuracy of the data, are of absolute importance. Vector data ideally consist of a building footprint polygon (or polyline) layer with height information embedded in the object structure or included in associated attribute tables. Using vector data with a full roof structure description (i.e. including objects such as chimneys etc.) makes it very complicated to derive wall areas, hence conversion to a raster dataset is recommended. The accuracy of the vector data becomes especially important where different building segments are located at the same position (e.g. two attached buildings). Those segments need to represent the difference in height between the two building roofs. This type of information is extremely rare and needs to be derived using geoprocessing techniques. A direct conversion of linear vector walls will result in an overestimation of wall areas (see Appendix in Lindberg et al., 2015). Here, a 4-directional  $3 \times 3$  kernel majority filter on a DSM is applied and then the differences between the original DSM and the raster produced by the filtering process are identified. By setting a threshold limit of the height that should represent a wall (e.g. 3 m), wall pixels are identified. The Urban Multi scale Environmental Predictor (UMEP) is used to derive all morphology parameters.  $f_{\text{roof}}$  is derived based on a high resolution ground and building DSM in conjunction with a DEM. Vector data can also be used, e.g. a polygon building footprint dataset.

### A2. Gap-filling

The outdoor air temperature ( $T_{\text{air}}$ ) is used as the base for creating a gap-filled surface temperature ( $T'_{\text{surf}}$ ) series. The method of cubic spline interpolation with not-a-knot end conditions is used (de Boor, 1978.). This type of interpolation uses a second derivative continuity at the joint points. It requires at least four consecutive surface temperature values, i.e. one diurnal period of satellite acquisition. First splines are constructed for the each of the remotely sensed surface element temperatures ( $T_{\text{surf spline}}$ ) and the *in-situ* measured outdoor air temperature ( $T_{\text{air spline}}$ ), respectively. For the outdoor air temperature ( $T_{\text{air}}$ ), only the values at the time of the surface temperature data points are used. Then the actual air temperature to the interpolated air temperature factor is calculated. Finally, that factor is used to scale the interpolated surface temperatures to construct high temporal resolution surface temperatures.

$$T'_{\text{surf}} = \frac{T_{\text{air}}}{T_{\text{air spline}}} T_{\text{surf spline}} \quad (6)$$

This gap filling method preserves the diurnal cycle as well as captures some of the shorter time scale variations from e.g. passing sparse clouds.

Alternatively, the Lindberg et al. (2008) method is used with the day split at sunrise and sunset. The outdoor air temperature ( $T_{\text{air}}$ ) is modified by a sine function of the difference between surface and air temperature which is set to zero at sunrise and sunset. The amplitude ( $a$ ) is a function of sun elevation angle ( $\alpha_s$ ).

$$T'_{\text{surf}} = a(\alpha_s) \sin\left(\frac{\pi}{2} \frac{t_{\text{day}} - t_{\text{elev}}}{t_{\text{mid}} - t_{\text{elev}}}\right) + T_{\text{air}} \quad (7)$$

To calculate the sine the time of day ( $t_{\text{day}}$ ), time of sunrise ( $t_{\text{elev}}$ ) and the time during the day with maximum outdoor air temperature ( $t_{\text{mid}}$ ) are used. Equation 7 is applicable for clear sky conditions and during daytime. With surface temperature available at the satellite overpass, it is possible to use the difference between air and surface temperature to calculate the sine function amplitude. With ground based surface temperature observations available methods can be explored to correct the gap-filling surface temperatures, but it will be dependent on location, e.g. if the sensors are observing a shaded surface or a sunlit surface.

### A3. Material characteristics

Each facet type (e.g., roof, ground, and wall) requires the surface material (e.g., gravel, tile, asphalt, concrete, etc.) to be specified (Table A1 and Table A2). These are obtained from a GIS database using EO, or other secondary geodata.

Furthermore, the depth and material composition of the active layer of each surface subcategory will be user defined. The material thermal conductivity and heat capacity of each layer will be integrated with respect to volume, resulting in an average heat capacity for the entire material volume. Finally, average thermal conductivity and heat capacity values for each surface type will be calculated by weighting subcategory values with respect to their surface coverage. The influence of material characteristics is further analysed and discussed in section 3.2.3.

**Table A1.** Material layer thicknesses and thermal properties for the Łódź and Basel ESTM calculations.

Element	Layer	Material	$\Delta x$ (m)	$k$ ( $W K^{-1} m^{-1}$ )	$\rho C$ ( $MJ K^{-1} m^{-3}$ )
roof	1	asphalt	0.03	0.74	1.9
	2	concrete	0.12	0.93	1.5
	3	insulation	0.05	0.06	0.07
wall	1-3	concrete & glass	0.1	0.95/0.93/0.93	1.6
internal	1-3	concrete	0.05	0.93	1.5
ground	1	asphalt & concrete	0.1	0.74	1.5
	2	asphalt	0.25	0.74	1.9
	3-4	sand & gravel	1.0/4.0	0.76/0.63	1.2

source: Offerle et al., 2005

**Table A2.** Material layer thicknesses and thermal properties for the London ESTM calculations.

Element	Layer	Material	$\Delta x$ (m)	$k$ ( $W K^{-1} m^{-1}$ )	$\rho C$ ( $MJ K^{-1} m^{-3}$ )
roof	1	concrete <sup>3</sup>	0.2 †	0.5 <sup>1</sup>	0.84 <sup>1</sup>
	2	insulation †	0.1 †	0.03 <sup>1</sup>	0.056 <sup>1</sup>
	3	wood †	0.05 †	0.14 <sup>1</sup>	0.78 <sup>1</sup>
wall (N, E, S)	1-3	concrete & glass <sup>2</sup>	0.05 <sup>1</sup>	0.31 <sup>1</sup> ‡	0.877 <sup>1</sup> ‡
internal	1-3	concrete †	0.035 <sup>2 4</sup>	0.5 <sup>1</sup>	1.0 <sup>1</sup>
ground	1	brick clay <sup>3</sup>	0.1 †	0.65 <sup>5 6</sup>	1.5 <sup>5 6</sup>
	2	concrete †	0.1 †	0.93 <sup>5 7</sup>	1.5 <sup>5 7</sup>
	3-4	sand & gravel †	1.0/3.0 <sup>7</sup>	0.63 <sup>5 7</sup>	1.2 <sup>5 7</sup>

source:

<sup>1</sup> Galezzi, 2010

<sup>2</sup> Behar, 2011

<sup>3</sup> Hogenhout, 2010

<sup>4</sup> Georgitsi, 2011

<sup>5</sup> Ashrae, 2013

<sup>6</sup> Mörtstedt and Hellsten, 1992

<sup>7</sup> Offerle et al., 2005

† estimation / guess

‡ theoretical